Geophysical & Astrophysical Fluid Dynamics

Publication details, including instructions for authors and subscription information:
http://www.tandfonline.com/loi/ggaf20

Surface semi-geostrophic dynamics in the ocean

G. Badin [a]

[a] Institut für Meereskunde, University of Hamburg, Hamburg, Germany

Version of record first published: 19 Nov 2012.

To cite this article: G. Badin (2012): Surface semi-geostrophic dynamics in the ocean, Geophysical & Astrophysical Fluid Dynamics, DOI:10.1080/03091929.2012.740479

To link to this article: http://dx.doi.org/10.1080/03091929.2012.740479

Geophysical and Astrophysical Fluid Dynamics
2012, 1–15, iFirst

Surface semi-geostrophic dynamics in the ocean

G. BADIN*†

Institut für Meereskunde,
University of Hamburg, Hamburg, Germany

(*Received 16 February 2012; in final form 6 September 2012*)

The surface quasi-geostrophic approximation is re-written in an oceanic context using the two-dimensional semi-geostrophic approximation. The new formulation allows to take into account the presence of out-of-balance flow features at scales comparable to or smaller than the Rossby radius of deformation and for small bulk Richardson numbers. Analytical solutions show that, while the surface quasi-geostrophic approximation tends to underestimate the buoyancy anomaly, the inclusion of finite Rossby number allows for larger values of the buoyancy anomaly at depth. The projection of the surface semi-geostrophic solution on the first baroclinic modes is calculated. The result of the projection is a functional form that decreases with the values of the Rossby number and toward smaller scales. Solutions for constant and exponential profile for the background potential vorticity are compared. Results of the comparison show that, in agreement with the results found for balanced flows, even for large Rossby number the exponential profile for the background potential vorticity retains smaller values for the buoyancy anomaly at depth than the solution found using a constant potential vorticity profile.

Keywords: Upper ocean and mixed layer processes; Fronts and jets

1. Introduction

In his seminal paper on geostrophic turbulence, Charney (1971) studied the statistical properties of finite amplitude turbulence in the quasi-geostrophic (QG) approximation under the assumption that the motion was restricted far away from boundaries. The opposite paradigm consists of finite amplitude turbulence for QG flows with constant, or zero, potential vorticity in the interior, but with buoyancy anomalies at the boundaries. The resulting approximation is also named surface quasi-geostrophic (SQG) approximation (Blumen 1978). Flows in the SQG approximation possess two invariants: the surface density variance and the depth integrated total energy, and they possess an inverse cascade of total energy at low wavenumbers and a direct cascade of

*Email: gualtiero.badin@zmaw.de
†Previously at: Program in Atmospheric and Oceanic Sciences, Princeton University, Princeton, NJ, USA.

Geophysical and Astrophysical Fluid Dynamics
ISSN 0309-1929 print/ISSN 1029-0419 online © 2012 Taylor & Francis
http://dx.doi.org/10.1080/03091929.2012.740479

density variance at the boundary at high wavenumbers (Blumen 1978, Pierrehumbert *et al*. 1994). In atmospheric dynamics problems, the SQG approximation has been used to study the dynamical properties of potential temperature anomalies on the tropopause (Juckes 1994), the asymmetry between cyclones and anticyclones (Hakim *et al*. 2002) and the shape of the tropopause spectra (Tulloch and Smith 2009). In ocean dynamics, the SQG approximation has been used, for example, to infer the interior dynamics of the ocean from the knowledge of sea surface temperature anomalies (LaCasce and Mahadevan 2006, Lapeyre and Klein 2006, Isern-Fontenet *et al*. 2008, Lapeyre 2009, Ferrari and Wunsch 2010, LaCasce 2012). Results show, however, that SQG tends to underestimate the buoyancy anomaly and current fields at depth. Employment of exponentially decaying stratification (LaCasce 2012) retains depth buoyancy anomaly values smaller than the observations. Moreover, in the SQG approximation buoyancy is cascaded by the full non-linear flow to small scales at the boundaries, creating filamentation and frontogenesis (Held *et al*. 1995, Lapeyre 2009). Dynamics associated with these processes, also referred to as submesoscale dynamics as they develop at scales smaller than the Rossby radius of deformation, are out of geostrophic balance, as they are locally characterised by the Rossby number $\epsilon = U/fL = \mathrm{O}(1)$, where U is the typical velocity of the flow, f is the Coriolis frequency, taken as constant, and L is the typical horizontal scale for the flow. Indicating with H the typical depth of the flow, $N^2 = b_z$ the buoyancy frequency, where $b = -g\rho/\rho_0$ is the buoyancy, ρ the potential density anomaly, ρ_0 a reference density and g the gravitational acceleration, it is possible to show that at scales comparable or smaller than the Rossby radius of deformation $R_d = NH/f$, the bulk Richardson number is

$$Ri = N^2H^2/U^2 = \epsilon^{-2}, \tag{1}$$

and thus $Ri = \mathrm{O}(1)$, demonstrating the importance of shear in submesoscale processes (Thomas *et al*. 2008). The breaking down of the QG approximation thus results in making the SQG approximation to lie in the contradiction of using balanced dynamics but to create dynamics that are out-of balance. The breaking down of the SQG approximation at scales smaller than the Rossby radius of deformation is also manifested by the poor representation that the approximation gives of the forward kinetic energy cascade at these scales (Capet *et al*. 2008). The aim of this note is to expand the surface dynamics to flows that are out-of-balance. To attain the expansion of the SQG approximation to out-of-balance flows, surface dynamics will be studied using the semi-geostrophic approximation (Hoskins and Bretherton 1972) in its two-dimensional formulation, in order to attain analytical solutions. The semi-geostrophic approximation was introduced for the study of frontogenesis in the atmosphere and it relies on the assumption of the validity of geostrophic balance across but not along fronts. An extension to three dimensions was introduced by Hoskins (1975). The problem of semi-geostrophic flows with potential vorticity constant in the interior has been solved for the Eady wave by Hoskins and Bretherton (1972) and Juckes (1998). In this note we aim to focus on the vertical structure of the solutions, in order to mimic the oceanographic problem to predict the motion in the interior of the ocean from the knowledge of the upper boundary condition. The problem here considered thus follows closely the analysis made by LaCasce (2012), but it differs on the fact that it makes use of the semi-geostrophic approximation and thus allows to consider flows that are out of balance.

2. Review of the semi-geostrophic approximation

Following Hoskins and Bretherton (1972) (see also Pedlosky (1987)), we consider a front with typical width l aligned in the zonal direction. The front has typical along-front length L. The typical along-front and cross-front velocities are, respectively, U and V, so that $UL \approx Vl$. We allow the dynamics to evolve on time scales longer than the inertial time scale, so that, if σ is the inverse time scale of the system, $\sigma/f \ll 1$. With the pressure term properly scaled, the non-dimensional equations of motions are thus

$$\epsilon \frac{\mathrm{D}u}{\mathrm{D}t} - v = -\frac{\partial p}{\partial x}, \qquad u = -\frac{\partial p}{\partial y}, \qquad \epsilon \frac{\partial p}{\partial z} = b, \tag{2a–c}$$

$$\frac{\partial u}{\partial x} + \frac{\partial v}{\partial y} + \frac{\partial w}{\partial z} = 0, \qquad \frac{\mathrm{D}b}{\mathrm{D}t} = 0, \tag{2d, e}$$

where $\epsilon = V(fl) = UL/(fl^2) = \mathrm{O}(1)$ and

$$\frac{\mathrm{D}}{\mathrm{D}t} = \frac{\partial}{\partial t} + u\frac{\partial}{\partial x} + v\frac{\partial}{\partial y} + w\frac{\partial}{\partial z}. \tag{2f}$$

In (2a–e), terms proportional to the cross-front Rossby number have been neglected. Equations (2a–e) satisfy the potential vorticity conservation

$$\frac{\mathrm{D}\Pi}{\mathrm{D}t} = 0 \qquad \text{with} \qquad \Pi = \omega_a \frac{\partial b}{\partial z} + \epsilon \frac{\partial u}{\partial z}\frac{\partial b}{\partial y}, \tag{3a, b}$$

where

$$\omega_a = 1 - \epsilon \frac{\partial u}{\partial y} \tag{3c}$$

is the absolute vorticity. Hoskins and Bretherton (1972) noted that, if expressed with a streamfunction, (3b) reduces to a Monge–Ampère elliptic equation, which is known to produce frontal discontinuities only at the boundaries (Heinz 1961). Using the thermal wind balance

$$\epsilon \frac{\partial u}{\partial z} = -\frac{\partial b}{\partial y}, \tag{4}$$

(3b) can also be written as

$$\Pi = \omega_a \frac{\partial b}{\partial z} - \epsilon^2 \left(\frac{\partial u}{\partial z}\right)^2. \tag{5}$$

Following Hoskins and Bretherton (1972), it is possible to decompose the flow into mean flow and perturbations, with the assumption that the perturbation fields only depend on the meridional and vertical directions and time $u = U(x) + u'(y, z, t)$, $v = V(y) + v'(y, z, t)$, $w = w'(y, z, t)$, $p = P(x, y, t) + p'(y, z, t)$, $b = b'(y, z, t)$ and that the mean flow satisfies readily (2a–e). In particular, Hoskins and Bretherton (1972) analyzed the cases of the mean flow representing a horizontal deformation field and a horizontally sheared flow. The perturbation equations for (2a–e)

are thus

$$\epsilon\frac{\mathrm{D}u'}{\mathrm{D}t} - v' = 0, \qquad u' = -\frac{\partial p'}{\partial y}, \qquad \epsilon\frac{\partial p'}{\partial z} = b', \tag{6a–c}$$

$$\frac{\partial v'}{\partial y} + \frac{\partial w'}{\partial z} = 0, \qquad \frac{\mathrm{D}b'}{\mathrm{D}t} = 0 \tag{6d, e}$$

with

$$\frac{\mathrm{D}}{\mathrm{D}t} = \frac{\partial}{\partial t} + (U + u')\frac{\partial}{\partial x} + (V + v')\frac{\partial}{\partial y} + w'\frac{\partial}{\partial z}. \tag{6f}$$

It can be noted that, since $\partial p'/\partial x = 0$, v' is entirely ageostrophic. The problem posed by (6a–f) is nonlinear. Following Hoskins and Bretherton (1972), it is possible to eliminate the nonlinearity of the problem by defining the transformation of co-ordinates

$$Y = y - \epsilon u, \qquad Z = z, \qquad T = t, \tag{7a–c}$$

where primes were dropped. The transformation (7a–c) defines a Legendre, or contact transformation and it has been studied for example, by Blumen (1980) and Purser (1999). Under the change of co-ordinates (7a–c), the partial derivatives for the time and spatial co-ordinates transform following the chain rule. In particular, the spatial co-ordinates transform as

$$\begin{pmatrix} \dfrac{\partial}{\partial y} \\ \dfrac{\partial}{\partial z} \end{pmatrix} = \begin{pmatrix} 1 - \epsilon\dfrac{\partial u}{\partial y} & 0 \\ -\epsilon\dfrac{\partial u}{\partial z} & 1 \end{pmatrix} \begin{pmatrix} \dfrac{\partial}{\partial Y} \\ \dfrac{\partial}{\partial Z} \end{pmatrix}. \tag{8}$$

It can be noted that the determinant of the transformation matrix is the absolute vorticity.

Defining the Bernoulli function $\epsilon\Psi$ [for a discussion on the scaling of the Bernoulli function, see Montgomery and Farrell (1990)] so that

$$b = \epsilon\frac{\partial \Psi}{\partial Z}, \tag{9}$$

the absolute vorticity in the transformed co-ordinates is

$$\omega_A = 1\big/(1 - \epsilon\Psi_{YY}). \tag{10}$$

A comparison between (3c) and (10) shows that in the transformed co-ordinates, the presence of the quantities at the denominator can give rise to very large values of vorticity. With (10), the potential vorticity (3b) in the transformed space is

$$Q = \omega_A \Psi_{ZZ} = \epsilon\frac{\Psi_{ZZ}}{(1 - \epsilon\Psi_{YY})} \qquad \text{or} \qquad \epsilon\Psi_{YY} + \frac{1}{Q}\epsilon\Psi_{ZZ} = 1. \tag{11a, b}$$

As noted by Hoskins (1976), (11b) differs from the QG equation for the potential vorticity due to the use of transformed co-ordinates and due to the presence of the

potential vorticity, rather than of the buoyancy frequency, at the denominator. On the horizontal boundaries, the boundary conditions are

$$\epsilon\Psi_Z = \begin{cases} b & \text{on} \quad Z = 0, \\ 0 & \text{on} \quad Z = -1, \end{cases} \tag{12}$$

where, at $Z = 0$, the conservation of buoyancy holds. Lateral boundary conditions must take into account that in the transformed reference frame the boundaries move with the flow. We thus set the Neumann boundary conditions

$$\lim_{Y\to\pm\infty} \epsilon\Psi_Y = 0 \qquad \text{or} \qquad \lim_{Y\to\pm\infty} \epsilon\Psi = g(Z). \tag{13a, b}$$

As Ψ is linked to the buoyancy anomaly, we can easily set $g(Z) = 0$. Alternatively, it can be seen that (11b)–(13b) supports two distinct limit solutions $g_1(Z)$ and $g_2(Z)$, suggesting that the model should support a frontal solution for finite Y. Notice that for the construction of the model, (11b)–(13b) cannot be used as prognostic equations to determine the depth of the motion, but can be used instead to determine the vertical profile of Ψ and b. If Q changes sign within the domain, (11b) is a non-homogeneous partial differential equation of mixed type. If $Q > 0$, (11b) is elliptic. If instead $Q < 0$, (11b) is hyperbolic. In particular, if Q is a linear function of Z, (11b) takes the form of a non-homogeneous Tricomi equation (Tricomi 1923). Mixed-type partial differential equations are found in fluid dynamics, for example in shock waves problems (Landau and Lifshitz 1987). In geophysical fluid dynamics, mixed-type partial differential equations appear, for example, in internal waves problems (Harlander and Maas 2006). In the ocean, Q can assume both positive and negative values, for example, due to the action of down-front winds which act to destroy potential vorticity (D'Asaro *et al.* 2011, Thomas 2005). Eventually, regions of negative potential vorticity develop symmetric instabilities which restore the potential vorticity to zero (Hoskins 1974, Rayleigh 1917, Taylor and Ferrari 2009). After differentiation by Z, (11b)–(13b) becomes a problem for the buoyancy anomaly

$$\frac{\partial^2 b}{\partial Y^2} + \frac{\partial}{\partial Z}\left(\frac{1}{Q}\frac{\partial b}{\partial Z}\right) = 0, \tag{14}$$

$$b = \begin{cases} b(Y) & \text{on} \quad Z = 0, \\ 0 & \text{on} \quad Z = -1, \end{cases} \tag{15}$$

$$\lim_{Y\to\pm\infty} b = 0. \tag{16}$$

Comparison between problems (6a)–(f) and (14)–(16) shows that in the latter, nonlinearities are retained only in the dependence of Q on b and in the transformation back into physical space.

3. Surface semi-geostrophic dynamics

We will now consider the case in which the potential vorticity Q is constant in the interior but the surface buoyancy anomaly is nonzero (Blumen 1978). Problem (11b)–(13b) thus constitutes a surface semi-geostrophic problem. Indicate with $\hat{\Psi}$ the

Fourier transform in Y of Ψ and after a separation of variables $\hat{\Psi} = \hat{b}\hat{\phi}$, where $\hat{\phi} = \hat{\phi}_k(Z)$, (11b) becomes

$$-k^2\epsilon\hat{\phi} + \frac{1}{Q}\epsilon\hat{\phi}_{ZZ} = 1, \tag{17}$$

with

$$\epsilon\hat{\phi}_Z = \begin{cases} 1 & \text{on} \quad Z = 0, \\ 0 & \text{on} \quad Z = -1, \end{cases} \tag{18}$$

and where k is a wavenumber. In dimensional variables $k^* = k/k_d$, where k_d is the wavenumber corresponding to the Rossby radius of deformation. As we are interested in scales that are equal or less than the Rossby radius of deformation, we will concentrate on the case $k \geq 1$. If we pose the background potential vorticity to be

$$Q = 1 - \frac{1}{Ri} \qquad \text{or, using (1),} \qquad Q = 1 - \epsilon^2, \tag{19a, b}$$

the problem posed by (17)–(19b) has the solution

$$\epsilon\hat{\phi} = \frac{1}{kL_1}\frac{\cosh[kL_1(Z+1)]}{\sinh(kL_1)}, \tag{20a}$$

where $L_1 = \sqrt{1-\epsilon^2} = \sqrt{Q}$. Equation (20a) differs from the finite-depth SQG solution considered, for example, by Tulloch and Smith (2006) due to the use of transformed co-ordinates, the contribution of ϵ and the presence of an inhomogeneous term in (17). The resulting buoyancy anomaly is

$$\epsilon\hat{\phi}_Z = \sinh[kL_1(Z+1)]\sinh(L_1k). \tag{20b}$$

The solutions (20a,b) can be transformed back into physical space. The reverse transformation can be obtained analytically (Andrews and Hoskins 1978, Blumen 1979, 1980) or with the aid of graphical methods. In this note we are, however, interested in the vertical structure of the solution and no such reverse transformation will be performed.

3.1. *Asymptotic behaviour of the solution*

It is interesting to analyse the asymptotic behaviour of the buoyancy anomaly $\epsilon\hat{\phi}_Z$ as a function of ϵ

$$\lim_{\epsilon\to 1}\epsilon\hat{\phi}_Z = 1 + Z, \tag{21a}$$

$$\lim_{\epsilon\to 0}\epsilon\hat{\phi}_Z = \sinh(k(Z+1))\sinh k. \tag{21b}$$

The result (21a) shows that for the Rossby number approaching unity, that is the value expected for out-of-balance flow, the vertical profile of the buoyancy anomaly decays linearly with depth and does not depend on the wavenumber k. Figure 1 shows the vertical profile of (21a) (full black line) and (21b) (dashed black line) for $k = 1$. Results show that the solution for $\epsilon \to 0$ (dashed black line) decays slower with depth than the

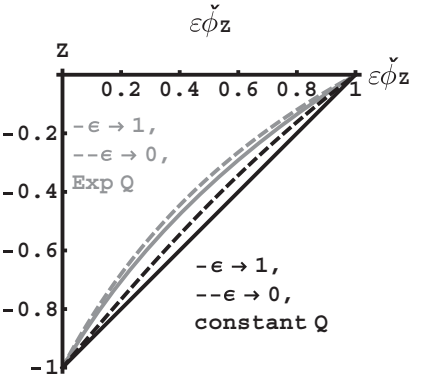

Figure 1. Vertical profile of the buoyancy anomaly $\epsilon\hat{\phi}_Z$ for the limit cases of $\epsilon \to 1$ (full line) and $\epsilon \to 0$ (dashed line) for constant (black lines) and exponential (grey lines) stratification.

solution for $\epsilon \to 1$ (full black line). The result (21a) thus suggests that the inclusion of out-of-balance dynamics would predict ocean interior buoyancy anomaly and velocity values larger than those found from the use of balanced dynamics. In the next sections, the sensitivity of the solution to the Rossby number and the wavenumber k will be discussed.

3.2. *Parametric dependence of the solution*

3.2.1. Streamfunction. The vertical structure of the streamfunction in the function of ϵ and k is shown in figure 2. Figure 2(a) shows the vertical structure of the streamfunction for $\epsilon = 0.1$ and $k = 1$ (full line), $k = 2$ (dashed line) and $k = 3$ (dot-dashed line). The three solutions have different slopes and intersect close to mid-depth, with $\epsilon\hat{\phi}_1(0) > \epsilon\hat{\phi}_2(0) > \epsilon\hat{\phi}_3(0)$, and vice-versa at $Z = -1$. The solutions also show zero crossings: this property of the solution is not present in the balanced SQG solution for depth limited flows, where solutions have the shape of exponential functions that tend to zero at depth (Tulloch and Smith 2006). For $\epsilon = 0.9$ (figure 2(b)), the solutions for different values of k appear instead as distinct curves, with similar slopes, not intersecting one another, and having positive values on all the vertical domain.

Figure 3(a) shows the dependence of the maximum value of the streamfunction, located at $Z = 0$, on ϵ for $k = 1$ (full line), $k = 2$ (dashed line) and $k = 3$ (dot-dashed line). The maximum value of the streamfunction appears to increase rapidly as ϵ increases, implying that, for the same sea surface buoyancy anomaly, the values of the velocities must be larger for the out-of-balance case. The increase of $\epsilon\hat{\phi}$ with ϵ is observed for all the wavenumbers, although the decrease is less pronounced for higher wavenumbers. The three solutions for different wavenumbers converge to zero as ϵ decreases. Finally, figure 3(b) shows the dependence of the maximum value of the streamfunction on k for $\epsilon = 0.9$ (full line), $\epsilon = 0.5$ (dashed line) and $\epsilon = 0$ (dot-dashed line). The maximum value of the streamfunction appears to decrease monotonically as k increases, thus towards smaller scales, with the solutions converging at zero. Results also show that $|\text{Max } \epsilon\hat{\phi}(\epsilon = 0.9) - \text{Max } \epsilon\hat{\phi}(\epsilon = 0.5)| > |\text{Max } \epsilon\hat{\phi}(\epsilon = 0.5) - \text{Max } \epsilon\hat{\phi}(\epsilon = 0.1)|$ for all

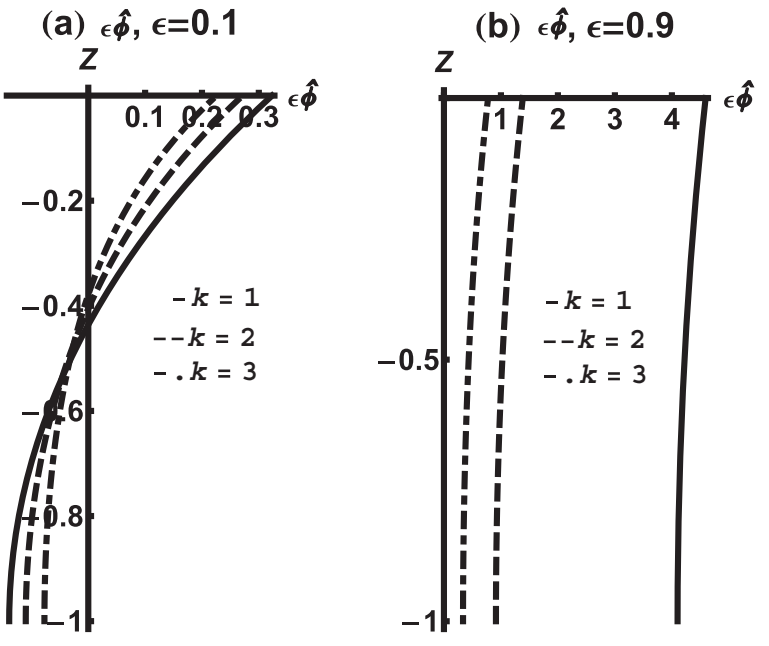

Figure 2. Vertical structure of $\epsilon\hat{\phi}$ for (a) $\epsilon = 0.1$ and (b) $\epsilon = 0.9$ for $k = 1$ (full line), $k = 2$ (dashed line) and $k = 3$ (dot-dashed line).

the values of k, suggesting a transition between the solutions out of balance ($\epsilon \to 1$) and the solutions closer to balance ($\epsilon \to 0$).

3.2.2. Buoyancy anomaly. The dependence of the buoyancy anomaly $\epsilon\hat{\phi}_Z$ on ϵ and k is shown in figure 4(a). The buoyancy anomaly is plotted along $Z = -0.5$, as the boundary conditions would set its nondimensional value automatically to 1 and 0, respectively, at the upper and lower boundary. The solution shows that the buoyancy anomaly increases monotonically with ϵ and decreases monotonically with k, with values tending asymptotically to zero. In detail, figure 4(b) shows the buoyancy anomaly profile as a function of k for $\epsilon = 0$ (dot-dashed line), $\epsilon = 0.5$ (dashed line) and $\epsilon = 0.9$ (full line). Results show that the buoyancy anomaly at mid-depth is larger as ϵ becomes larger for all the wavenumbers. The differences between the three solutions are not monotonic with k. Figure 4(c) shows that the difference $\epsilon\hat{\phi}_Z(\epsilon = 0.9) - \epsilon\hat{\phi}_Z(\epsilon = 0.1)$ has a maximum for $k = 5$. Figure 4(b) also shows that, along $Z = -0.5$, $|\epsilon\hat{\phi}_Z(\epsilon = 0.9) - \epsilon\hat{\phi}_Z(\epsilon = 0.5)| > |\epsilon\hat{\phi}_Z(\epsilon = 0.5) - \epsilon\hat{\phi}_Z(\epsilon = 0.1)|$ for all the values of k, suggesting also a transition between the solutions out of balance and the solutions closer to balance for the buoyancy anomaly. Finally, figure 4(d) shows the buoyancy anomaly profile as a function of ϵ for $k = 1$ (full line), $k = 2$ (dashed line) and $k = 3$ (dot-dashed line). Results show that the buoyancy anomaly at mid-depth is larger for the lower modes for all the values of the Rossby number. As observed in figure 2(b), as $\epsilon \to 1$ the streamfunction tends to have the same vertical structure and the same slope. This result is reflected in figure 4(d), where, as $\epsilon \to 1$, the three solutions tend to converge to the same value.

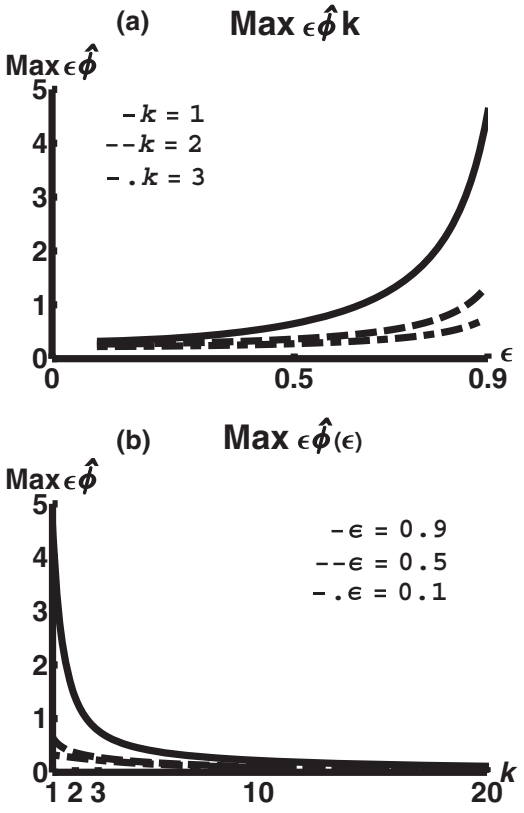

Figure 3. Maximum value of $\epsilon\hat{\phi}$, located at $Z=0$, (a) in the function of ϵ, for $k=1$ (full line), $k=2$ (dashed line) and $k=3$ (dot-dashed line) and (b) in the function of k, for $\epsilon=0.9$ (full line), $\epsilon=0.5$ (dashed line) and $\epsilon=0.1$ (dot-dashed line).

3.3. *Projection on baroclinic modes*

To find the interior modes, problem (17)–(19b) can be modified to

$$-k^2\hat{\varphi}+\frac{1}{1-\epsilon^2}\hat{\varphi}_{ZZ}=\frac{1}{\epsilon}, \tag{22}$$

$$\epsilon\hat{\varphi}_Z=\begin{cases}0 & \text{on} \quad Z=0,\\ 0 & \text{on} \quad Z=-1,\end{cases} \tag{23}$$

where $\hat{\varphi}$ is the Fourier transform of the interior streamfunction. The problem (22), (23b) has the solution

$$\hat{\varphi}_n(Z)=\mathrm{Re}\left\{\mathrm{e}^{\mathrm{i}n\pi Z}+\mathrm{e}^{-\mathrm{i}n\pi Z}+\frac{1-\epsilon^2}{\epsilon n^2\pi^2}\right\}, \tag{24}$$

where $(1-\epsilon^2)k=\mathrm{i}\pi n$ and $n\in\mathbb{N}^+$. Using (24), it is possible to find the projection of the surface semi-geostrophic streamfunction into the baroclinic modes. The projection is

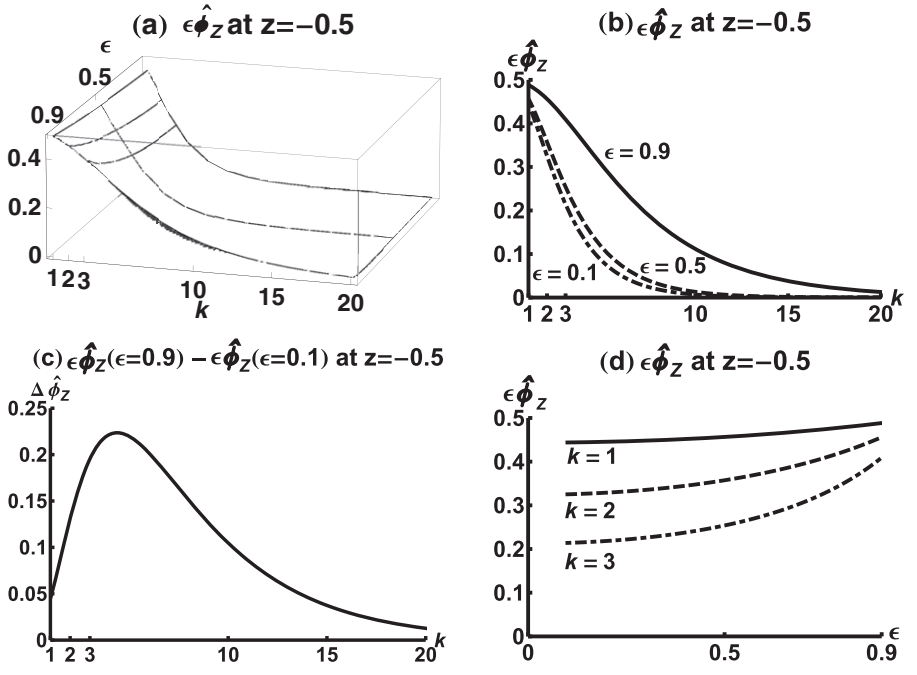

Figure 4. (a) Buoyancy anomaly $\epsilon\hat{\phi}_Z$ at $Z=-0.5$ in the function of ϵ and k. (b) Sections of (a) along $\epsilon=0.9$ (full line), $\epsilon=0.5$ (dashed line) and $\epsilon=0.1$ (dot-dashed line). (c) $\epsilon\hat{\phi}_Z(\epsilon=0.9)-\epsilon\hat{\phi}_Z(\epsilon=0.1)$ at $Z=-0.5$ in the function of k. (d) Sections of (a) along $k=1$ (full line), $k=2$ (dashed line) and $k=3$ (dot-dashed line).

defined by the functional

$$C[\epsilon,k,n]=\frac{\int_{-1}^{0}\epsilon^2\hat{\phi}\hat{\varphi}_n\,\mathrm{d}Z}{\int_{-1}^{0}\left|\epsilon\hat{\varphi}_n\right|^2\mathrm{d}Z} \tag{25a}$$

which can be solved analytically and has the solution

$$C[\epsilon,k,n]=\frac{(-1)^{2n}\epsilon n^2\pi^2\left[2k^2n^2\pi^2+\epsilon\left(k^2+n^2\pi^2\right)-\epsilon^3k^2\right]}{k^2[(1-\epsilon^2)k^2+n^2\pi^2][1+2\epsilon^2(n^4\pi^4-1)+\epsilon^4]}. \tag{25b}$$

Figure 5 shows the values of (25b) for varying ϵ for the first two baroclinic modes and for different values of k. Results show that for all the baroclinic modes the square of the projection of the surface semi-geostrophic solution decreases as ϵ increases. In detail, for $k=1$, the square of the projection on the first baroclinic mode ($n=1$, full black line) varies from $C^2\,[\epsilon=0.1,\,k=1,\,n=1]=0.42$ to $C^2\,[\epsilon=0.9,\,k=1,\,n=1]=0.03$. For $k=2$, instead, the square of the projection on the first baroclinic mode (dashed black line) varies from $C^2\,[\epsilon=0.1,\,k=2,\,n=1]=0.24$ to $C^2\,[\epsilon=0.9,\,k=2,\,n=1]=0.014$. At smaller scales ($k=3$), the square of the projection on the first baroclinic mode (dot-dashed black line) varies from $C^2\,[\epsilon=0.1,\,k=3,\,n=1]=0.13$ to $C^2\,[\epsilon=0.9,\,k=3,\,n=1]=0.01$. For different values of k, the square of the projection on the first baroclinic mode thus tends to converge to the same value as ϵ increases. This result is in agreement with the observed result that for high ϵ the solutions for the surface

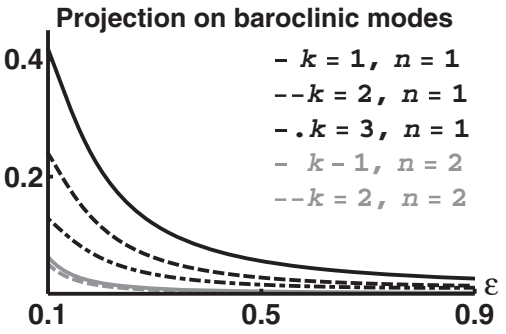

Figure 5. Dependence on ϵ of the projection on the first baroclinic mode ($n=1$) for $k=1$ (full black line), $k=2$ (dashed black line), $k=3$ (dot-dashed black line) and on the second baroclinic mode ($n=2$) for $k=1$ (full grey line) and $k=2$ (dashed grey line).

semi-geostrophic problem tend to assume the same vertical structure. For the second baroclinic mode ($n=2$), the square of the projection of the surface semi-geostrophic solution exhibits a slower decrease with ϵ and a faster convergence to the same value for different values of k. In detail, for $k=1$ the square of the projection on the second baroclinic mode (full grey line) varies from $C^2\,[\epsilon=0.1,\, k=1,\, n=2]=0.25$ to $C^2\,[\epsilon=0.9,\, k=1,\, n=2]=0.04$, while for $k=2$ the square of the projection on the second baroclinic mode (dashed grey line) varies from $C^2\,[\epsilon=0,\, k=2,\, n=2]=0.23$ to $C^2\,[\epsilon=0.9,\, k=2,\, n=2]=0.03$. For the third baroclinic mode ($n=3$, not shown) at scales comparable to the Rossby radius of deformation ($k=1$), the functional varies from $C^2\,[\epsilon=0.1,\, k=1,\, n=3]=0.12$ to $C^2\,[\epsilon=0.9,\, k=1,\, n=3]=0.02$. Thus, for fixed ϵ, the square of the projection decreses monotonically going to smaller scales (larger k) and to higher baroclinic modes. However, for fixed ϵ, the difference of the values of the square of the projection for different k and different n is larger for smaller values of ϵ.

Figure 6 shows the behaviour of the square of the projection on the first three baroclinic modes in the function of k in the semi-log scale. For $\epsilon=0.1$ (figure 6(a)), results show that the square of the projection of the solution on the baroclinic modes decrease monotonically. It is interesting to note that the square of the projection on the first baroclinic mode (full black line) decays faster than the square of the projection of the solution on the higher baroclinic modes: for $k>7$ and $k>12$ the square of the projection on the first baroclinic mode assumes smaller values than the square of the projection on the second (dashed black line) and third (dot-dashed line) baroclinic modes, respectively. For $\epsilon=0.9$ (figure 6(b)), results show instead that the square of the projection of the solution on the first baroclinic mode dominates instead on the square of the projection of the higher baroclinic modes for all k.

4. Exponentially decaying potential vorticity

If Q is a function of depth, and in particular if it decays exponentially with depth,

$$Q=\left(1-\frac{1}{Ri}\right)e^{Z}, \tag{26}$$

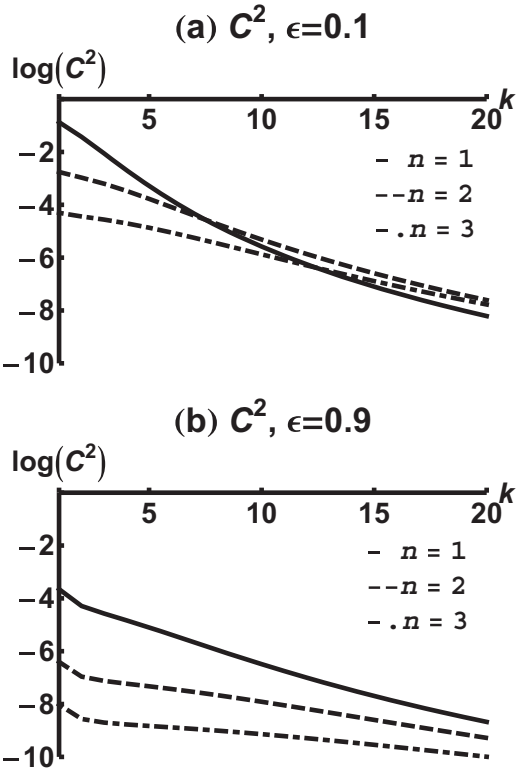

Figure 6. Dependence on the wavenumber k of the square of the projection on the first ($n=1$, full black line), second ($n=2$, dashed black line) and third ($n=3$, dot-dashed black line) baroclinic modes for (a) $\epsilon=0.1$ and (b) $\epsilon=0.9$ in the semi-log scale.

after a Fourier transform and with the use of (1), (14) becomes the Bessel equation

$$\frac{e^{-Z}}{1-\epsilon^2}\left\{\left[\epsilon\hat{\phi}_Z\right]_{ZZ}-\left[\epsilon\hat{\phi}_Z\right]_Z\right\}-k^2\epsilon\hat{\phi}_Z=0 \tag{27}$$

with boundary conditions

$$\epsilon\hat{\phi}_Z=\begin{cases}1 & \text{on} \quad Z=0,\\ 0 & \text{on} \quad Z=-1.\end{cases} \tag{28}$$

The problem (27), (28) has the solution

$$\epsilon\hat{\phi}=\mathrm{e}^{Z/2}\frac{\left[\mathrm{I}_1(2kL_2)\,\mathrm{K}_1(2k\mathrm{e}^{Z/2}L_1)-\mathrm{I}_1(2k\mathrm{e}^{Z/2}L_1)\,\mathrm{K}_1(2kL_2)\right]}{\left[\mathrm{I}_1(2kL_2)\,\mathrm{K}_1(2kL_1)-\mathrm{I}_1(2kL_1)\,\mathrm{K}_1(2kL_2)\right]}, \tag{29}$$

where I_1 and K_1 are, respectively, hyperbolic Bessel functions of the first and second kind and $L_2=\sqrt{(1-\epsilon^2)}/\mathrm{e}$. As for the case with constant potential vorticity, it is instructive to look at the asymptotic solutions of (29):

$$\lim_{\epsilon\to 1}\epsilon\hat{\phi}_Z=\frac{k^2\mathrm{e}^{Z+1}-1}{\mathrm{e}-1} \tag{30a}$$

and

$$\lim_{\epsilon\to 0}\epsilon\hat{\phi}_Z = \mathrm{e}^{Z/2}\frac{\left[\mathrm{I}_1(2/\sqrt{\mathrm{e}})\,\mathrm{K}_1(2\mathrm{e}^{Z/2}) - \mathrm{I}_1(2\mathrm{e}^{Z/2})\,\mathrm{K}_1(2/\sqrt{\mathrm{e}})\right]}{\left[\mathrm{I}_1(2/\sqrt{\mathrm{e}})\,\mathrm{K}_1(2) - \mathrm{I}_1(2)\,\mathrm{K}_1(2/\sqrt{\mathrm{e}})\right]}. \tag{30b}$$

Differently from the case with constant potential vorticity, (30a) retains the k dependence and decays exponentially with depth. Figure 1 shows the vertical profile of (30a) (full grey line) and (30b) (dashed grey line) for $k=1$. Results also show that for exponential potential vorticity the solution for $\epsilon\to 0$ (dashed grey line) decays slower with depth, although the difference is less pronounced than for the case of constant potential vorticity. Comparison between the solutions for constant potential vorticity (black lines) with the solutions for exponential potential vorticity (grey lines) shows that, even for $\epsilon\to 1$, the exponential stratification profile tends to underestimate the buoyancy anomaly at depth. The underestimation of the buoyancy anomaly at depth is in agreement with the results found for balanced flows by LaCasce (2012). It should be noted that the vertical profile (26) has an e-folding depth equal to unity: if a smaller e-folding depth would have been employed, the solutions for the exponential profile would have resulted in a larger underestimation of the buoyancy anomaly profile at depth.

5. Discussion

To take into account the presence of out-of-balance flows, characterised by O(1) Rossby and Richardson numbers, the surface quasi-geostrophic approximation was re-written for an oceanic context using the semi-geostrophic approximation. The inclusion of the effects of the large Rossby number allows for larger values of the buoyancy anomaly at depth. This feature of the surface semi-geostrophic approximation thus seems to correct the underestimation of the balanced subsurface currents and buoyancy anomaly observed by LaCasce and Mahadevan (2006) and Lapeyre and Klein (2006) in numerical simulations and data analysis, and by LaCasce (2012) in analytical solutions obtained making use of realistic stratification. The projection of the surface semi-geostrophic solution to the first baroclinic modes can be expressed as a functional form that decreases with the values of the Rossby number and as smaller scales are approached. Results show that even for the small Rossby number, at scales comparable to the Rossby radius of deformation, the first baroclinic mode accounts for 42% of the total vertical structure of the flow. For large values of the Rossby number, at scales comparable to the Rossby radius of deformation, the first baroclinic mode accounts instead for 3% of the total vertical structure of the flow. Numerical simulations of mixed layer instabilities show that small-scale out-of-balance instabilities tend to project in the barotropic mode (Badin *et al*. 2011), making them able to mix tracers in the ocean interior. The problem of the vertical distribution of energy between the barotropic and baroclinic modes is reflected in the problem of detecting ocean currents through sea surface altimetry. While sea surface altimetry seem to be able to detect motion occurring at the first baroclinic mode (Wunsch 1997), the increase of the barotropic component of the flow for the larger Rossby number might affect our power to detect the flow from satellites. The results found here are based on a number of

approximations: in the real ocean, frontal features actively change the potential vorticity in the interior through the subduction of low potential vorticity (Thomas 2008). Further, both the balanced SQG solutions, and the solutions derived here, are locked by the upper boundary condition, that in the real ocean is determined by the presence of a surface mixed layer. We suggest that a surface solution could then be found assuming that the surface buoyancy anomaly must match the buoyancy anomaly at the base of the mixed layer, where the Rossby number can still assume large values. Alternatively, a surface solution can be matched to an interior solution (e.g., Garrett and Munk 1972). A comparison with data or with numerical simulations is thus required to test whether the solutions can represent a good approximation of the real ocean.

Acknowledgements

I would like to thank A. Mahadevan and A. Tandon for invaluable discussions, F. Crisciani for reading an early draft of this manuscript and two anonymous referees for constructive comments. The Tricomi problem was pointed out to me by A. Mahadevan and L. Mahadevan. This study was partially funded by the following grants: NASA Grant NNX10AE93G, ONR Grant N00014-09-1-0179, DOE Grant DE-SC0005189 and NSF Grant AGS-1144302.

References

Andrews, D.G. and Hoskins, B.J., Energy spectra predicted by semi-geostrophic theories of frontogenesis. *J. Atmos. Sci.* 1978, **35**, 509–512.

Badin, G., Tandon, A. and Mahadevan, A., Lateral mixing in the pycnocline by baroclinic mixed layer eddies. *J. Phys. Oceanogr.* 2011, **41**, 2080–2101.

Blumen, W., Uniform potential vorticity flow: part I. Theory of wave interactions and two-dimensional turbulence. *J. Atmos. Sci.* 1978, **35**, 774–783.

Blumen, W., Unstable nonlinear evolution of an Eady wave in time-dependent basic flows and frontogenesis. *J. Atmos. Sci.* 1979, **36**, 3–11.

Blumen, W., The geostrophic coordinate transformation. *J. Atmos. Sci.* 1980, **38**, 1100–1105.

Capet, X., Klein, P., Hua, B.L., Lapeyre, G. and McWilliams, J.C., Surface kinetic energy transfer in surface quasi-geostrophic flows. *J. Fluid Mech.* 2008, **604**, 165–174.

Charney, J.G., Geostrophic turbulence. *J. Atmos. Sci.* 1971, **28**, 1087–1095.

D'Asaro, E., Lee, C., Rainville, L., Harcourt, R. and Thomas, L., Enhanced turbulence and energy dissipation at ocean fronts. *Science* 2011, **332**, 318–322.

Ferrari, R. and Wunsch, C., The distribution of eddy kinetic and potential energies in the global ocean. *Tellus* 2010, **62**, 92–108.

Garrett, C. and Munk, W., Space-time scales of internal waves. *Geophys. Fluid Dyn.* 1972, **2**, 225–264.

Hakim, G.J., Snyder, C. and Muraki, D.J., A new surface model for cyclone-anticyclone asymmetry. *J. Atmos. Sci.* 2002, **59**, 2405–2420.

Harlander, U. and Maas, L.R.M., Two alternatives for solving hyperbolic boundary value problems of geophysical fluid dynamics. *J. Fluid Mech.* 2006, **588**, 331–351.

Heinz, E., Interior estimates for solutions of elliptic Monge–Ampere equations. in *Proceedings of the Symposium of Pure Mathematics, Vol. IV, Partial Differential Equations*, pp. 149–155, 1961. (American Mathematical Society: Providence, RI, USA).

Held, I., Pierrehumbert, R., Garner, S. and Swanson, K., Surface quasi-geostrophic dynamics. *J. Fluid Mech.* 1995, **282**, 1–20.

Hoskins, B.J., The role of potential vorticity in symmetric stability and instability. *Q.J.R. Meteorol. Soc.* 1974, **100**, 480–482.

Hoskins, B.J., The geostrophic momentum approximation and the semi-geostrophic equations. *J. Atmos. Sci.* 1975, **32**, 233–242.
Hoskins, B.J., Baroclinic waves and frontogenesis. Part I: introduction and Eady waves. *Q.J.R. Meteorol. Soc.* 1976, **102**, 103–122.
Hoskins, B.J. and Bretherton, F., Atmospheric frontogenesis models: mathematical formulation and solutions. *J. Atmos. Sci.* 1972, **29**, 11–37.
Isern-Fontenet, J., Lapeyre, G., Klein, P., Chapron, B. and Hecht, M.W., Three-dimensional reconstruction of oceanic mesoscale currents from surface information. *J. Geophys. Res.* 2008, **113**, C09005.
Juckes, M., Quasigeostrophic dynamics of the tropopause. *J. Atmos. Sci.* 1994, **51**, 2756–2768.
Juckes, M.N., Baroclinic instability of semi-geostrophic fronts with uniform potential vorticity I: An analytic solution. *Q.J.R. Meteorol. Soc.* 1998, **124**, 2227–2257.
LaCasce, J.H., Surface quasigeostrophic solutions and baroclinic modes with exponential stratification. *J. Phys. Oceanogr.* 2012, **42**, 569–580.
LaCasce, J.H. and Mahadevan, A., Estimating subsurface horizontal and vertical velocities from sea-surface temperature. *J. Mar. Res.* 2006, **64**, 695–721.
Landau, L.D. and Lifshitz, E.M., *Fluid Mechanics. Course of Theoretical Physics*, 2d ed., Vol. 6, 1987. (Oxford, UK: Butterworth-Heinemann).
Lapeyre, G., What vertical mode does the altimeter reflect? On the decomposition in baroclinic modes and on a surface-trapped mode. *J. Phys. Oceanogr.* 2009, **39**, 2857–2874.
Lapeyre, G. and Klein, P., Dynamics of the upper oceanic layers in terms of surface quasigeostrophy theory. *J. Phys. Oceanogr.* 2006, **36**, 165–179.
Montgomery, M.T. and Farrell, B.F., Dry surface frontogenesis arising from interior potential vorticity perturbations in a semigeostrophic model. *J. Atmos. Sci.* 1990, **47**, 2837–2852.
Pedlosky, J., *Geophysical Fluid Dynamics*, 2nd ed., 728pp, 1987. (New York, USA: Springer).
Pierrehumbert, R.T., Held, I.M. and Swanson, K.L., Spectra of local and nonlocal two-dimensional turbulence. *Chaos, Solitons, Fractals* 1994, **4**, 1111–1116.
Purser, R., Legendre-transformable semigeostrophic theories. *J. Atmos. Sci.* 1999, **56**, 2522–2535.
Rayleigh, L., On the dynamics of revolving fluids. *Proc. R. Soc. Lond. A* 1917, **93**, 148–154.
Taylor, J.R. and Ferrari, R., On the equilibration of a symmetrically unstable front via a secondary shear instability. *J. Fluid Mech.* 2009, **622**, 103–113.
Thomas, L., Destruction of potential vorticity by winds. *J. Phys. Oceanogr.* 2005, **35**, 2457–2466.
Thomas, L., Formation of intrathermocline eddies at ocean fronts by wind-driven destruction of potential vorticity. *Dyn. Atmos. Oceans* 2008, **45**, 252–273.
Thomas, L.N., Tandon, A. and Mahadevan, A., Submesoscale processes and dynamics. In *Ocean Modeling in an Eddying Regime*, edited by M. Hecht and H. Hasumi, Vol. 177, pp. 17–38, 2008. (Washington, DC: American Geophysical Union), Geophysical Monograph Series.
Tricomi, G.F., Sulle equazioni lineari alle derivate parziali di 2 ordine di tipo misto. *Rend. Atti Accad. Naz. Lincei* 1923, **14**, 134–247.
Tulloch, R. and Smith, K.S., A new theory for the atmospheric energy spectrum: Depth-limited temperature anomalies at the tropopause. *Proc. Nat. Acad. Sci.* 2006, **103**, 14 690–14 694.
Tulloch, R. and Smith, K.S., Quasigeostrophic turbulence with explicit surface dynamics: application to the atmospheric energy spectrum. *J. Atmos. Sci.* 2009, **66**, 450–467.
Wunsch, K., The vertical partition of oceanic horizontal kinetic energy. *J. Phys. Oceanogr.* 1997, **27**, 1770–1794.